J. Earth Planet. Sci. Nagoya Univ., Vol. 56, 13 to 29, 2009

A preliminary report on the geochemistry of amphibolites from the Chuncheon area in the Gyeonggi massif, Korea

Kazuhiro SUZUKI[1]*, Daniel J. DUNKLEY[2], Izumi KAJIZUKA[1] and Ueechan CHWAE[3]

[1]The Center for Chronological Research, Nagoya University, Chikusa-ku, Nagoya 464-8602, Japan
[2]National Institute of Polar Research, 10-3 Midoricho, Tachikawa, Tokyo 190-8513, Japan
[3]Korea Institute of Geoscience and Mineral Resources, 92 Gwahang-no, Yuseong-gu, Daejon, Korea
(Received December 4, 2009 / Accepted December 30, 2009)

ABSTRACT

Amphibolites in the Gubongsan Group at Chuncheon, South Korea have garnet-bearing and garnet-free assemblages: garnet+tschermakitic hornblende+quartz+plagioclase+biotite (garnet amphibolite), relict garnet+edenitic hornblende+plagioclase+quartz+biotite (relict garnet-bearing amphibolite), edenitic hornblende+plagioclase+quartz+biotite and tschermakitic to edenitic hornblende+plagioclase+chlorite+quartz+biotite. The garnet relics are extensively embayed and surrounded by coronas of plagioclase+edenitic hornblende. Whole-rock compositions of amphibolite samples are equivalent to basaltic protoliths with MORB-like characteristics. Garnet-free, chlorite-bearing amphibolite is the most magnesian, with an $Fe^{2+}/(Fe^{2+}+Mg)$ value of 0.26. Graphical representations of whole-rock and mineral compositions show that individual mineral assemblages approach chemical equilibrium and define distinct compositional volumes in the A (Al_2O_3+Fe_2O_3-Na_2O-K_2O) – C (CaO) – F (FeO) – M (MgO) tetrahedron. The A component is critical in determining the stability of the garnet-bearing assemblage, which occurs above a threshold that decreases at higher Fe/(Fe+Mg) values. As a result, small variations in bulk composition can produce differing mineral assemblages. Whole-rock Sr concentrations are significantly depleted in garnet amphibolite, whereas values in relict garnet-bearing and garnet-free amphibolite match typical basaltic compositions. The depletion may be attributable to leaching via fluids released by dehydration reactions and the prograde breakdown of Sr hosts, such as plagioclase and epidote.

INTRODUCTION

The Gyeonggi massif is located in the middle Korean Peninsula and is bounded by the Okcheon belt to the south and by the Imjingang fold belt to the north (Fig. 1). The massif comprises garnetiferous quartzofeldspathic, granitic and pelitic granulites, psammitic and pelitic sub-granulitic gneisses, along with subordinate amounts of amphibolite and crystalline calcareous rocks (Lee, 1987; Lee and Cho, 1995; Sagong *et al.*, 2003). Amphibolites provide valuable information on the tectonic processes

* Corresponding author, e-mail: suzuki@nendai.nagoya-u.ac.jp

that accompanied metamorphism and orogenesis. Oh *et al.* (2005) and Kim *et al.* (2006) reported eclogitic remnants, mostly retrogressed to garnet amphibolite, from the Hongseong and Bibong areas in the southwestern Gyeonggi massif. Sajeev *et al.* (2009) reported high-pressure garnet amphibolite from the Imjingang belt. These

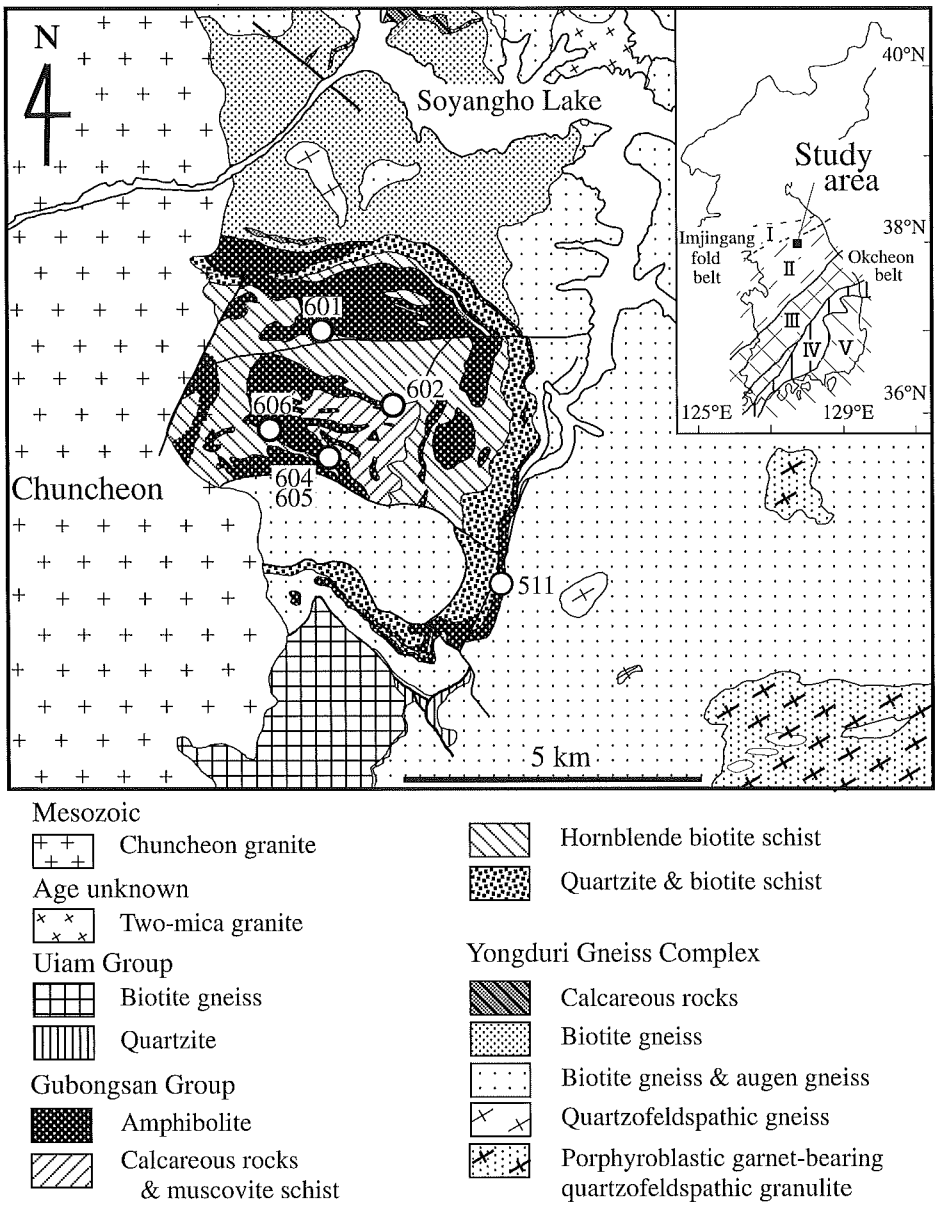

Fig. 1 Geological map of the Chuncheon area (simplified from Park *et al.*, 1974), showing locations of analyzed samples. The insert is a simplified tectonic map of Korea (after Lee, 1987). I: Imjingang fold belt, II: Gyeonggi massif, III: Okcheon belt, IV: Yeongnam massif, V: Gyeongsang basins.

studies suggested that garnet amphibolites formed under high-pressure conditions which cannot be reached in a continental crust with a normal thickness of 30–40 km, and that their formation must be related to plate collisions. Chemical aspects of amphibolites also provide information on pre-orogenic tectonic environments. Oh *et al.* (2004) suggested that the Baekdong metabasite in the Hongseong area originated from island arc tholeiite. Otherwise, limited attention has been drawn to the geochemical aspect of amphibolites within the Gyeonggi massif.

The Chuncheon area hosts one of the largest amphibolite bodies in the Gyeonggi massif. Amphibolites occur as conformable layers or discordant dykes within a supracrustal sequence of quartzite, lime-silicate rock and mica schist, juxtaposed over a Mesoproterozoic granulite complex. The protolith of the amphibolite was suggested as tholeiitic basalt that erupted in an intracontinental rift (Kwon *et al.*, 1995). However, independent evidence of a rift tectonic setting has not been reported from the Mesoproterozoic granulite complex in the Chuncheon area. In this paper, we will present XRF analyses of garnetiferous and garnet-free amphibolites from the Chuncheon area, and will examine the relationships between whole-rock composition and mineral assemblages.

GEOLOGY

The Chuncheon area is underlain mainly by high-grade metamorphic rocks that are grouped into the Yongduri Gneiss Complex, the Gubongsan Group and the Uiam Group (Park *et al.*, 1974; Fig. 1). The Yongduri Gneiss Complex comprises porphyroblastic garnet-bearing quartzofeldspatic (granitic) granulite, coarse-grained quartzofeldspathic gneiss, augen gneiss and biotite gneiss. The Gubongsan Group includes amphibolite, calcareous rocks, hornblende-biotite schist, mica schist and quartzite. The Uiam Group comprises a lower quartzite horizon of 30 to 100 m in thickness and an upper horizon of biotite gneiss. The Gubongsan Group overlies the Yongduri Gneiss Complex (Park *et al.*, 1974) and is overthrust by the Uiam Group with an E-NE vergence. All lithological units were intruded by the Chuncheon granite at around 210 Ma (Jin *et al.*, 1993).

Amphibolites in the Gubongsan Group have been classified into three types: (1) concordant and schistose layers of either sedimentary or igneous origin, commonly intercalated with calc-silicate layers; (2) concordant and massive layers of possible igneous origin; and (3) discordant dykes intruding metasedimentary rocks (Lee and Cho, 1995). Lee and Cho (1995) further separated amphibolite lithologies into garnet-bearing and garnet-free assemblages. The metamorphic pressures and temperatures of amphibolite formation are in the ranges of 5.5–10.6 kbar and 615–714°C (Lee and Cho, 1995). Variation in pressure and temperature estimates within samples is comparable to that between localities. This is contrary to the simple (and most likely) metamorphic scenario, where structurally-concordant amphibolites throughout the Gubongsan Group formed during the same regional event at consistent pressures and temperatures. As a result, other factors that may influence thermobarometry need to be assessed, such as the control of whole-rock chemistry on mineral assemblages.

The age of the Yongduri Gneiss Complex is poorly constrained. Suzuki *et al.* (2002)

reported electron-microprobe analyses of monazite in porphyroblastic garnet-bearing quartzofeldspathic gneiss; most Th-U-Pb data sets yielded 1100–1850 Ma apparent ages, possibly recording a Mesoproterozoic metamorphic event. However, mylonitized garnet-free quartzofeldspathic gneiss contains no Mesoproterozoic monazite, instead yielding a CHIME age of 236±34 Ma.

The protolith age of amphibolite in the Gubongsan Group was estimated at 852±48 Ma by the Sm-Nd whole-rock isochron method (Kwon *et al.*, 1995). The age of the amphibolite-facies metamorphism has been variously estimated as Devonian (391±75 Ma; Sm-Nd garnet-feldspar-whole rock isochron, Sagong *et al.*, 2003), or Triassic (224±14 Ma and 239±94 Ma; in-situ SIMS analysis of titanite, Kim *et al.*, 2008). The metamorphic age of the Uiam Group has been estimated at 240±21 Ma by the CHIME dating of monazite in biotite gneiss that occurs with sillimanite-K-feldspar paragneiss (Suzuki *et al.*, 2002). The latter age estimates for the metamorphism of the supracrustal sequence are similar to that obtained for mylonitized quartzofeldspathic gneiss of the Yongduri Gneiss Complex. Similar age relationships were reported from the Hwacheon area, about 10 km northwest of the Chuncheon area, and were interpreted as the result of thrusting of a hot Permian metamorphic complex over the Mesoproterozoic granulite complex (Suzuki, 2009). Following this model, the Gubongsan Group and the Uiam Group may represent allochthons in the Yongduri Gneiss Complex.

SAMPLE DESCRIPTION

Eleven samples of amphibolite were collected from five outcrops in the Gubongsan Group (Fig. 1). Sample 511 represents a ca. 1 m-thick schistose layer within a calc-silicate dominated sequence. The other samples were taken from concordant layers of schistose amphibolite that are mostly greater than 5 m thick. Most samples (601, 602A, 605B, 605T, 606A, 606B and 606C) contain porphyroblastic garnet, and three samples (511, 602B and 604B) are free from garnet. Garnet amphibolite consists mainly of Hbl+Grt+Qtz+Pl+Bt (mineral abbreviations after Kretz, 1983). Garnet-free amphibolite comprises Hbl+Pl+Qtz+Bt (samples 511 and 604B) and Hbl+Pl+Qtz+Chl+Bt (sample 602B). Primary chlorite occurs only in sample 602B in textural equilibrium with hornblende, plagioclase and quartz, and attains ca. 3% by mode. Hornblende ranges in mode from 50 to 75%, plagioclase from 10 (in garnet amphibolite) to 30%, and garnet from trace amounts (in sample 605A) to 25% (in sample 606A). Ilmenite, ulvöspinel, pyrrhotite, titanite, apatite and zircon occur as accessory phases. Secondary chlorite, prehnite, calcite and epidote occur in negligibly small amounts in most samples. Retrograde actinolite is rarely developed on hornblende margins. Symplectic intergrowths of fine-grained plagioclase and actinolitic hornblende develop around garnet porphyroblasts in some garnet amphibolites.

Schistosity is mainly defined by flattened grains of hornblende, whereas garnet, when present, occurs as 1–6 mm wide poikilitic porphyroblasts. In samples 601, 602A, 606A, 606B and 606C, garnet porphyroblasts overprint the foliation, and enclose quartz, hornblende and ilmenite. Fig. 2A shows a garnet porphyroblast in sample 606A, which contains inclusions that define a foliation that has been rotated relative to the dominant foliation in the matrix. The top and bottom margins of the grain are replaced to a

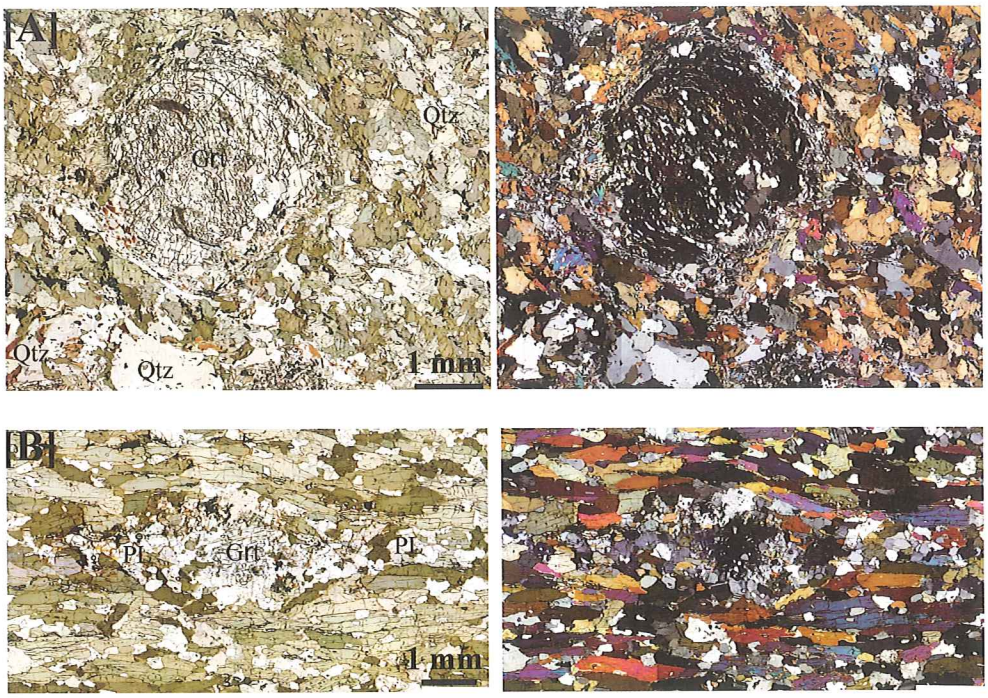

Fig. 2 Single polar (left) and crossed polar (right) photomicrographs of porphyroblastic garnet in 606A garnet amphibolite [A] and relict garnet with a recrystallized retrograde corona of plagioclase and hornblende in 605B relict garnet-bearing amphibolite [B]. Most colorless grains are quartz and plagioclase in sub-equal amounts in sample 606A, whereas in sample 605B plagioclase is more abundant.

minor degree by fine-grained plagioclase and hornblende. The texture suggests that garnet grew during an earlier stage of deformation and has survived later deformation. In contrast, garnet in samples 605A, 605B and 605T is only preserved as minor relics of porphyroblasts, pervasively replaced by coronas that mainly consist of plagioclase, hornblende, and minor pyrrhotite and/or iron oxides. In sample 605B (Fig. 2B), the corona recrystallized and attenuated into tails extending parallel to the matrix foliation, indicating garnet breakdown before or during late-stage deformation.

WHOLE-ROCK CHEMISTRY

Whole-rock compositions were analyzed with a SHIMADZU XRF1800 wavelength dispersive sequential X-ray fluorescence spectrometer with an end-window 4 kW Rh X-ray tube at the Center for Chronological Research, Nagoya University. Individual samples of around 100 to 200 g were broken up into small pieces by pounding with a hammer against a steel plate before conversion into small chips in a steel mortar. Powdering to 200-mesh was done in an agate mortar. After drying in an oven heated to 110°C for 24 hours, powders were mixed with anhydrous lithium tetraborate (0.7 g sample plus 6 g flux for analysis of major elements, and 2 g sample plus 3 g flux for

trace elements) and fused in a $Pt_{90}Au_{10}$ crucible in an electric furnace. The fusion was repeated at least twice to ensure homogenization of the glass bead. The analytical procedure followed those described in Morishita and Suzuki (1993) and Yamamoto and Morishita (1997). The tube voltage was 40 kV, and the tube current was 70 mA for major elements, and 95 mA for the trace elements V, Cr, Co, Ni, Cu, Zn, Rb, Sr, Y, Zr, Nb, Ba, Pb and Th. Spectral interferences such as RbKβ on YKα, YKα on NbKα, TiKβ on VKα, VKβ on CrKα, and SrKβ on ZrKα were corrected for. The detection limits were 10 ppm for Ba and 0.5–2 ppm for other trace elements at the 2σ confidence level. Ferrous-to-ferric iron was determined by conventional titration with 0.1 mol potassium permanganate solution. The analytical results are listed in Table 1.

Table 1. XRF analyses of garnet amphibolites (Grt), relic garnet-bearing amphibolites (rGrt) and garnet-free amphibolites from the Gubongsan Group of the Gyeonggi massif in the Chuncheon area, Korea.

Sample No.	511	601	602A	602B	604B	605A	605B	605T	606A	606B	606C
		Grt	Grt			rGrt	rGrt	rGrt	Grt	Grt	Grt
SiO_2	49.75	49.93	48.39	49.20	49.73	49.06	49.34	50.79	49.20	49.97	51.43
TiO_2	2.31	1.26	1.28	0.90	1.70	2.12	2.14	1.57	3.19	2.87	2.94
Al_2O_3	13.76	15.43	14.14	14.26	13.79	12.99	13.03	12.48	13.51	12.59	12.85
Fe_2O_3	1.58	0.68	1.49	2.85	2.18	2.11	2.61	2.17	2.71	1.76	2.57
FeO	10.74	10.03	13.05	6.43	10.72	11.91	11.49	13.44	12.80	13.48	12.01
MnO	0.17	0.16	0.25	0.16	0.26	0.20	0.20	0.25	0.20	0.23	0.22
MgO	6.54	8.76	8.05	10.23	6.07	5.89	5.94	5.39	5.54	5.39	4.91
CaO	9.36	8.58	10.33	8.40	11.32	10.45	10.36	9.73	10.22	8.51	9.32
Na_2O	3.45	2.30	1.39	2.45	1.72	2.34	2.32	1.97	0.73	0.47	0.53
K_2O	0.35	0.73	0.40	1.38	0.19	0.88	0.79	0.75	0.83	1.86	1.05
P_2O_5	0.25	0.13	0.09	0.15	0.17	0.20	0.21	0.14	0.31	0.31	0.28
Ig. Loss	1.89	1.71	0.89	2.88	2.14	1.20	1.31	1.19	0.56	2.14	1.48
Total	100.15	99.70	99.75	99.29	99.99	99.35	99.74	99.87	99.80	99.58	99.59
$\frac{Fe^{2+}}{(Fe^{2+}+Mg)}$	0.48	0.39	0.48	0.26	0.50	0.53	0.52	0.58	0.56	0.58	0.58
V	338.0	306.2	348.4	240.6	313.6	388.8	391.4	410.4	529.3	355.2	479.6
Cr	78.3	260.2	204.4	368.4	77.4	47.6	52.2	53.6	67.1	74.7	61.5
Co	64.5	58.8	50.5	66.6	52.3	57.3	58.6	0.0	54.2	50.6	55.1
Ni	54.1	48.2	73.3	128.5	36.8	29.1	30.1	23.0	51.9	36.4	50.6
Cu	22.9	0.0	10.6	13.3	268.7	179.3	198.5	197.0	46.0	86.8	30.3
Zn	146.4	84.2	153.1	83.8	84.7	101.8	104.3	108.4	120.8	136.4	105.9
Rb	7.5	39.5	10.7	43.5	2.6	27.4	23.0	15.8	25.9	104.4	42.5
Sr	147.2	52.7	48.2	363.4	143.6	267.8	258.2	135.4	37.6	20.5	33.9
Y	27.1	25.3	24.6	20.0	29.8	29.2	29.3	41.8	44.5	43.3	42.2
Zr	160.6	101.4	77.6	90.6	108.1	125.6	127.6	102.2	242.4	208.2	218.9
Nb	10.9	4.6	3.2	2.6	5.5	8.7	8.2	3.8	13.2	11.8	11.9
Ba	31.8	35.3	19.6	520.0	127.9	103.4	93.1	66.2	94.8	140.3	150.0
Pb	2.1	8.2	4.4	4.2	0.2	1.8	1.0	2.6	3.3	2.5	2.7
Th	0.6	1.5	1.1	2.8	0.9	1.0	0.6	0.5	2.8	0.8	0.6

The whole-rock chemistry of all samples approximates typical basaltic compositions, with SiO_2 contents from 48.39 to 51.43 wt.%. They have moderate to high contents of TiO_2 (0.90 to 3.19 wt.%) and low contents of Al_2O_3 (12.48 to 15.43 wt.%). There is a larger variation in the FeO (7.92–13.56 wt.%) and MgO (4.91 to 10.23 wt.%) contents. The $Fe^{2+}/(Fe^{2+}+Mg)$ values range 0.39 to 0.58 with an exceptionally low value of 0.26 for chlorite-bearing sample 602B. The CaO content varies from 8.40 to 11.32 wt.%, whereas Na_2O and K_2O contents have large variations of 0.53–3.45 wt.% and 0.19–1.86 wt.%, respectively. The garnet-bearing amphibolites tend to be lower (0.47–1.39 wt.%) in Na_2O than the garnet-free amphibolites (1.72–3.45 wt.%).

The V content, ranging from 240 to 530 ppm, is positively correlated with $Fe^{2+}/(Fe^{2+}+Mg)$. The most magnesian sample 602B has the highest Cr and Ni contents, at 368 and 128 ppm, respectively. The Cr and Ni contents decrease steeply with increasing $Fe^{2+}/(Fe^{2+}+Mg)$ up to a value of 0.5, and then remain around 60 and 45 ppm, respectively. The Sr content ranges from 135 to 363 ppm for garnet-free and relict garnet-bearing amphibolites, whereas for garnet amphibolites it is below 52 ppm.

MINERAL CHEMISTRY

Chemical compositions of constituent minerals are listed in Tables 2 and 3. The analyses were obtained using a JCXA-733 electron-microprobe equipped with four wavelength dispersive spectrometers at the Center for Chronological Research, Nagoya University. The instrument operating conditions were 15 kV accelerating voltage, 15 nA probe current and 2 μm probe diameter. The raw X-ray intensity data were converted into concentrations through the Bence and Albee's procedure (Bence and Albee, 1968) using the α-factor table provided by Kato (2005) and α-factors determined on synthetic glass samples of simple compositions. Total iron in minerals is assumed to be ferrous in Tables 2 and 3.

Garnet amphibolite 602A and garnet-free amphibolite 602B were collected from different horizons in a single outcrop. Garnet has relatively high CaO. The Al and Si-cations approach 2 and 3 per 12 oxygens, respectively, with an insignificant andradite component. The almandine content is almost constant throughout grains (57.4–58.2%). Spessartine content is slightly lower in grain interiors (6.1%) than in margins (6.1–7.7%). Pyrope content decreases at margins from 11.3 to 10.0%. Grossular content is higher in grain interiors (25.2–24.5%) than in margins (23.4%). Amphiboles vary from tschermakitic hornblende to magnesio-hornblende in both samples, following the nomenclature of Leake *et al.* (1997). In garnet amphibolite 602A, Al, Ca and Na+K contents are around 2.50, 1.80 and 0.48 per 23 oxygens, respectively. Amphibole in garnet-free amphibolite 602B has lower Al (2.11) and Ca (1.75) contents and higher Na+K (0.72–0.82) contents, approaching the composition of pargasitic hornblende. The Ti contents are lower in garnet amphibolite than in garnet-free amphibolite (0.08–0.19). Plagioclase in garnet amphibolite varies from bytownite in grain cores to labradorite in rims (An_{61}). Plagioclase grains in garnet-free amphibolite display continuous zoning under the microscope, with core-to-rim variation from bytownite (An_{82}) through labradorite to oligoclase (An_{24}). Minor secondary chlorite surrounding garnet in 602A is rich in Al and Fe, whereas primary chlorite in sample 602B is low in

Table 2. Electron microprobe analyses of constituent minerals in 602A garnet amphibolite and 602B garnet-free amphibolite collected from the same outcrop. Grt-R and Pl-R represent the rim of garnet and plagioclase grains, respectively. Total Fe is given as FeO.

602A	Grt	Grt	Grt-R	Hbl	Hbl	Hbl	Pl	Pl	Pl	Pl-R	Bt	Ilm	Chl
SiO_2	37.51	37.37	37.41	43.63	43.52	44.62	46.61	46.79	49.15	52.42	32.51	0.00	25.53
TiO_2	0.17	0.06	0.17	0.69	0.81	0.95	0.00	0.00	0.00	0.00	3.05	52.35	0.12
Al_2O_3	21.28	21.28	21.25	14.11	14.37	12.08	33.93	33.66	32.55	30.00	16.28	0.00	20.75
FeO	26.17	26.49	26.64	16.92	15.95	17.37	0.21	0.13	0.11	0.05	24.47	44.27	28.11
MnO	2.74	3.20	3.49	0.21	0.15	0.28	0.00	0.00	0.00	0.00	0.24	2.89	0.33
MgO	2.90	2.60	2.81	9.35	9.88	9.01	0.00	0.00	0.04	0.00	10.13	0.00	13.10
CaO	8.97	8.71	8.40	11.35	11.38	11.15	17.10	16.95	15.48	12.56	0.09	0.00	0.14
BaO	0.00	0.00	0.00	0.00	0.00	0.00	0.00	0.00	0.00	0.00	0.10	0.00	0.00
Na_2O	0.00	0.00	0.00	1.37	1.46	1.32	1.76	1.78	2.75	4.39	0.00	0.00	0.00
K_2O	0.00	0.00	0.03	0.48	0.59	0.54	0.02	0.00	0.00	0.03	7.54	0.00	0.10
H_2O	0.00	0.00	0.00	1.91	1.92	1.89	0.00	0.00	0.00	0.00	4.47	0.00	10.65
Total	99.74	99.70	100.19	100.01	99.70	99.25	99.62	99.32	100.07	99.18	98.88	99.51	99.06
O=	12	12	12	23	23	23	8	8	8	8	22	3	28
Si	2.980	2.979	2.972	6.481	6.422	6.671	2.150	2.162	2.244	2.387	5.142	0.000	5.426
Ti	0.010	0.003	0.010	0.078	0.089	0.107	0.000	0.000	0.000	0.000	0.363	0.999	0.019
Al	1.992	1.999	1.989	2.463	2.500	2.128	1.845	1.834	1.751	1.610	3.035	0.000	5.198
Fe^{2+}	1.739	1.766	1.770	2.096	1.968	2.172	0.008	0.005	0.004	0.002	3.237	0.939	4.997
Mn	0.185	0.216	0.235	0.026	0.019	0.035	0.000	0.000	0.000	0.000	0.032	0.062	0.060
Mg	0.343	0.309	0.332	2.063	2.175	2.009	0.000	0.000	0.003	0.000	2.388	0.000	4.150
Ca	0.764	0.744	0.715	1.801	1.798	1.786	0.845	0.840	0.757	0.613	0.015	0.000	0.031
Ba	0.000	0.000	0.000	0.000	0.000	0.000	0.000	0.000	0.000	0.000	0.006	0.000	0.000
Na	0.000	0.000	0.000	0.394	0.420	0.382	0.157	0.160	0.243	0.388	0.000	0.000	0.000
K	0.000	0.000	0.003	0.091	0.111	0.103	0.001	0.000	0.000	0.002	1.521	0.000	0.028

602B	Hbl	Hbl	Hbl	Act	Pl	Pl	Pl	Pl	Pl	Pl-R	Bt	Usp	Chl
SiO_2	47.47	43.81	43.22	53.61	47.14	47.31	53.09	54.70	56.14	61.85	39.11	0.10	28.88
TiO_2	0.75	1.73	1.45	0.75	0.00	0.00	0.00	0.00	0.00	0.00	2.09	10.24	0.00
Al_2O_3	7.82	12.32	12.26	4.58	32.96	33.00	29.36	28.10	27.26	23.52	13.96	1.27	18.34
FeO	9.89	9.60	11.95	8.66	0.55	0.36	0.39	0.36	0.30	0.26	14.83	81.45	15.13
MnO	0.22	0.21	0.24	0.25	0.00	0.00	0.00	0.00	0.00	0.00	0.18	1.04	0.23
MgO	17.31	15.61	14.52	18.00	0.00	0.00	0.00	0.00	0.00	0.00	15.66	1.13	23.86
CaO	11.41	11.05	11.20	11.85	16.52	16.35	11.95	10.48	9.55	5.06	0.00	0.66	0.00
BaO	0.00	0.00	0.00	0.00	0.00	0.00	0.00	0.09	0.00	0.14	0.26	0.00	0.00
Na_2O	1.63	2.33	2.10	0.63	2.02	2.13	4.58	5.41	5.94	8.16	0.11	0.00	0.00
K_2O	0.42	0.89	0.63	0.22	0.03	0.00	0.22	0.32	0.35	0.83	9.03	0.00	0.20
H_2O	2.04	1.91	1.93	2.02	0.00	0.00	0.00	0.00	0.00	0.00	3.81	0.00	11.22
Total	99.05	99.46	99.49	100.57	99.22	99.15	99.59	99.47	99.52	99.80	99.08	95.89	97.90
O=	22	23	23	23	8	8	8	8	8	8	22	4	28
Si	6.596	6.370	6.349	7.510	2.184	2.190	2.416	2.485	2.538	2.758	5.815	0.090	5.827
Ti	0.079	0.189	0.161	0.079	0.000	0.000	0.000	0.000	0.000	0.000	0.234	0.330	0.000
Al	1.281	2.111	2.122	0.756	1.800	1.800	1.574	1.505	1.453	1.236	2.446	0.064	4.362
Fe^{2+}	1.149	1.167	1.467	1.014	0.021	0.014	0.015	0.014	0.011	0.010	1.844	2.920	2.553
Mn	0.026	0.026	0.029	0.030	0.000	0.000	0.000	0.000	0.000	0.000	0.022	0.038	0.038
Mg	3.586	3.383	3.180	3.760	0.000	0.000	0.000	0.000	0.000	0.000	3.471	0.072	7.179
Ca	1.699	1.723	1.763	1.779	0.820	0.811	0.583	0.510	0.463	0.242	0.000	0.030	0.000
Ba	0.000	0.000	0.000	0.000	0.000	0.000	0.000	0.002	0.000	0.002	0.015	0.000	0.000
Na	0.440	0.657	0.598	0.171	0.182	0.192	0.404	0.477	0.520	0.705	0.033	0.000	0.000
K	0.074	0.164	0.118	0.040	0.002	0.000	0.013	0.019	0.020	0.047	1.713	0.000	0.052

Table 3. Electron microprobe analyses of constituent minerals in 601A garnet amphibolite, 605B relic garnet-bearing amphibolite and 606A garnet amphibolite. Grt-R represents the rim of garnet grain. The marks -C and -S indicate minerals in corona and symplektite around garnet porphyroblast.

601	Grt	Grt-R	Hbl	Hbl	Pl	Pl	Pl	Bt	Ilm	605B	Grt	Grt-R	Hbl
SiO_2	38.09	37.71	45.24	43.47	49.10	53.34	60.42	35.75	0.00		37.60	37.74	43.76
TiO_2	0.00	0.00	0.81	0.67	0.00	0.00	0.00	2.10	52.96		0.24	0.20	1.10
Al_2O_3	21.41	21.38	14.45	15.04	32.25	29.15	24.51	17.45	0.05		21.03	21.15	10.14
FeO	28.11	27.95	12.49	12.43	0.05	0.35	0.18	16.77	44.99		22.95	22.93	18.49
MnO	1.47	2.01	0.15	0.14	0.00	0.00	0.00	0.10	1.83		4.96	4.45	0.28
MgO	5.07	3.93	11.96	12.16	0.00	0.00	0.00	13.35	0.00		1.45	1.53	9.90
CaO	5.39	6.21	11.00	11.35	15.23	11.78	6.21	0.12	0.00		11.91	11.74	11.68
BaO	0.00	0.00	0.00	0.00	0.00	0.00	0.00	0.00	0.00		0.00	0.00	0.00
Na_2O	0.00	0.00	1.73	1.82	2.91	4.86	8.10	0.77	0.00		0.00	0.00	1.60
K_2O	0.00	0.00	0.44	0.41	0.00	0.00	0.00	8.37	0.00		0.00	0.00	1.07
H_2O	0.00	0.00	1.96	1.93	0.00	0.00	0.00	3.75	0.00		0.00	0.00	1.87
Total	99.54	99.19	100.23	99.42	99.54	99.48	99.42	98.53	99.83		100.14	99.74	99.89
O=	12	12	23	23	8	8	8	22	3.00		12	3	23
Si	3.005	3.001	6.528	6.359	2.252	2.427	2.703	5.397	0.00		2.987	2.999	6.606
Ti	0.010	0.000	0.088	0.073	0.000	0.000	0.000	0.238	1.01		0.014	0.012	0.125
Al	1.991	2.005	2.457	2.593	1.074	1.563	1.292	3.106	0.00		1.968	1.981	1.804
Fe^{2+}	1.855	1.866	1.507	1.520	0.002	0.013	0.007	2.117	0.94		1.525	1.524	2.335
Mn	0.098	0.135	0.019	0.018	0.000	0.000	0.000	0.013	0.04		0.334	0.300	0.036
Mg	0.597	0.467	2.573	2.652	0.000	0.000	0.000	3.004	0.00		0.172	0.182	2.228
Ca	0.456	0.530	1.701	1.754	0.749	0.574	0.297	0.019	0.00		1.014	1.000	1.890
Ba	0.000	0.000	0.000	0.000	0.000	0.000	0.000	0.000	0.00		0.000	0.000	0.000
Na	0.000	0.000	0.483	0.516	0.259	0.429	0.703	0.226	0.00		0.000	0.000	0.469
K	0.000	0.000	0.081	0.077	0.000	0.000	0.000	1.612	0.00		0.000	0.000	0.206

605B	Hbl	Hbl-C	Pl	Pl-C	Bt	606A	Grt	Grt-R	Hbl	Hbl-S	Pl	Pl-S	Bt
SiO_2	44.89	41.71	61.83	59.68	35.46		38.26	37.66	42.17	44.82	47.08	48.55	36.47
TiO_2	1.03	1.21	0.00	0.00	3.19		0.09	0.18	1.01	1.00	0.00	0.00	4.16
Al_2O_3	10.43	12.72	23.90	25.37	15.27		21.50	21.25	14.63	10.48	34.11	32.84	15.29
FeO	18.84	20.96	0.10	0.06	22.62		26.32	26.60	17.50	19.22	0.11	0.15	20.77
MnO	0.27	0.49	0.00	0.00	0.20		0.28	1.05	0.09	0.11	0.00	0.00	0.03
MgO	9.30	6.89	0.00	0.00	9.63		2.51	2.44	8.45	8.88	0.00	0.00	10.50
CaO	10.93	11.24	5.23	7.00	0.16		11.64	10.93	11.43	11.41	17.12	15.87	0.02
BaO	0.00	0.00	0.00	0.00	0.12		0.00	0.00	0.00	0.00	0.00	0.00	0.21
Na_2O	1.32	1.42	8.51	7.50	0.05		0.00	0.00	1.31	1.03	1.76	2.50	0.17
K_2O	0.92	1.41	0.20	0.26	7.96		0.00	0.00	0.97	0.74	0.00	0.00	9.08
H_2O	1.89	1.85	0.00	0.00	3.64		0.00	0.00	1.88	1.88	0.00	0.00	3.74
Total	99.82	99.90	99.77	99.87	98.30		100.60	100.11	99.44	99.57	100.18	99.91	100.44
O=	23	23	8	8	22		12	12	23	23	8	8	22
Si	6.740	6.385	2.748	2.664	5.513		2.998	2.981	6.333	6.747	2.157	2.223	5.521
Ti	0.117	0.139	0.000	0.000	0.373		0.005	0.011	0.114	0.113	0.000	0.000	0.474
Al	1.845	2.294	1.252	1.335	2.798		1.986	1.983	2.590	1.859	1.842	1.772	2.727
Fe^{2+}	2.365	2.683	0.004	0.002	2.942		1.725	1.761	2.198	2.420	0.004	0.006	2.629
Mn	0.034	0.064	0.000	0.000	0.026		0.019	0.070	0.011	0.014	0.000	0.000	0.004
Mg	2.082	1.573	0.000	0.000	2.231		0.293	0.287	1.892	1.993	0.000	0.000	2.369
Ca	1.759	1.843	0.249	0.335	0.027		0.977	0.971	1.839	1.841	0.840	0.778	0.004
Ba	0.000	0.000	0.000	0.000	0.007		0.000	0.000	0.000	0.000	0.000	0.000	0.013
Na	0.384	0.421	0.733	0.649	0.015		0.000	0.000	0.381	0.299	0.156	0.222	0.049
K	0.177	0.276	0.011	0.015	1.579		0.000	0.000	0.185	0.141	0.000	0.000	0.754

Al and rich in Mg, reflecting differences in whole-rock composition and/or the stage of growth (Table 1).

Samples 601 and 606A represent magnesian and ferriferous garnet amphibolites, respectively. In sample 601, garnet grains have a core composition of $Alm_{61.7}Sps_{3.3}Prp_{19.8}Grs_{15.2}$ with a retrogressive rim of $Alm_{62.2}Sps_{4.5}Prp_{15.6}Grs_{17.7}$ (Table 2). The grossular content increases from the core to the rim along with increasing in Fe/Mg. In ferriferous sample 606A, garnet cores and rims have similar compositions of $Alm_{57.3}Sps_{0.6}Prp_{9.7}Grs_{32.4}$. The grossular content is distinctly higher in sample 606A than in sample 601. Amphibole is tschermakitic hornblende and ferro-tschermakitic hornblende in samples 601 and 606A, respectively.

Sample 605B represents the relict garnet-bearing amphibolite. The relict garnet is rich in Mn with compositions of around $Alm_{50.1}Sps_{11.0}Prp_{5.6}Grs_{33.3}$. Amphibole in the corona around relict garnet is ferroan pargasitic to edenitic hornblende with a Na+K value of around 0.7, whereas that in the matrix is ferro-edenitic hornblende. Plagioclase is andesine in the corona and oligoclase in the matrix.

DISCUSSION

Tectonic setting of amphibolite protoliths

Element mobility during post-magmatic alteration and metamorphism is the major problem for the discrimination of tectonic settings for protoliths from geochemical data. In general, it has been observed that most major elements and many trace elements, mainly large ion lithophile elements, are mobile during hydrothermal alteration (*e.g.* Floyd and Winchester, 1975). However, the effects of metamorphism on whole-rock Al, Ti, high field strength elements (*e.g.* Th, Nb, Zr, Nb), rare earth elements, and other elements such as Cr and Ni are often regarded as less significant (*e.g.* Ludden *et al.*, 1982; Kerric *et al.*, 1999; Alirezaei and Cameron, 2002).

Amphibolite samples are plotted on the TiO_2-MnO-P_2O_5 discrimination diagram (Mullen, 1983) in Fig. 3A. Data spread from the IAT field through the MORB field to the OIT field. In the Zr/Y vs. Zr diagram (Fig. 3B, Pearce and Norry, 1979), compositions lie within the MORB and WPB fields. However, in the Ti-Zr-Y diagram (Pearce and Cann, 1973, Fig. 3C), the samples fall mainly in the field of mixed affinity between MORB and IAT. These rule out a within-plate basalt origin, but do not distinguish between ocean floor and volcanic arc origins. On the basis of the Ti-Zr-Y relationship, Oh *et al.* (2004) classified the protoliths of metabasites in the Hongseong area as island arc tholeiite (open circles in Fig. 3C). However, in the V-Ti diagram (Shervais, 1982, Fig. 3D), Gubongsan Group samples occupy the MORB field. An ocean floor origin is therefore favored over an island arc origin for the protoliths of amphibolite in the Chuncheon area.

Phase relationships in amphibolites

The whole-rock compositions of amphibolite samples are plotted on the conventional ACF (A=Al_2O_3+Fe_2O_3-Na_2O-K_2O, C=CaO and F=FeO+MnO+MgO) projection (Fig. 4A). The compositional range is limited but consistent with variations in mineral assemblage. The Al-rich and Ca-poor samples (601, 602A, 606A, 606B and 606C),

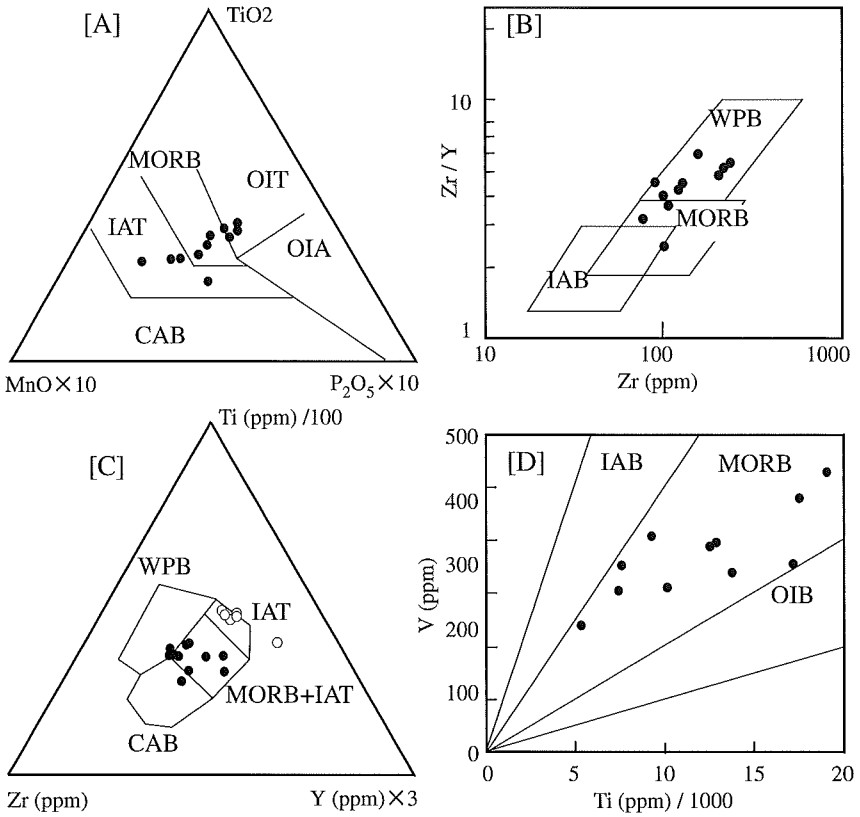

Fig. 3 Plots of whole-rock compositions on discrimination diagrams of: [A] Mullen (1983), [B] Pearce and Norry (1979), [C] Pearce and Cann (1973), and [D] Shervais (1982). MORB: mid oceanic ridge basalt, OIT: ocean island tholeiite, OIA: ocean island alkali basalt, IAT: island arc tholeiite, CAB: calc-alkaline basalt, WPB: within plate basalt and IAB: island arc basalt. Open circles in C represent metabasites of Oh *et al.* (2004).

excluding the anomalously magnesian sample 602B, show a stable association of garnet and tschermakitic hornblende. Lower Al samples are garnet-free (511 and 604B) or contain minor relict garnet in coronas of plagioclase and ferro-edenitic hornblende (605A, 605B and 605T).

The phase relations can be examined in the ACFM (F=FeO+MnO, M=MgO) tetrahedron with excess quartz and H_2O. Fig. 4B shows the projection of phase relationships from anorthite onto a plane that contains the F-M edge of the ACFM tetrahedron and that is parallel to the A-C edge. Garnet amphibolites 601, 602A and 606A contain tschermakitic hornblende, with Fe/(Fe+Mg) variations matching whole-rock variations, as would be expected in a well-equilibrated assemblage under a restricted range of pressures and temperatures. Similar variations are present in biotite and garnet; in addition, the grossular content of garnet decreases with increasing Fe/(Fe+Mg). Garnet stability is restricted to samples with higher (A-C)/(F+M) and Fe/(Fe+Mg) values (Fig. 4b). Magnesian 602B sample has a Pl+Hbl+Chl+Bt assemblage, which

may be attributable to the disappearance of the Grt-Hbl tie line on the ACF diagram (Fig. 4A), and the appearance of a Pl-Chl tie line, in more magnesian whole-rock

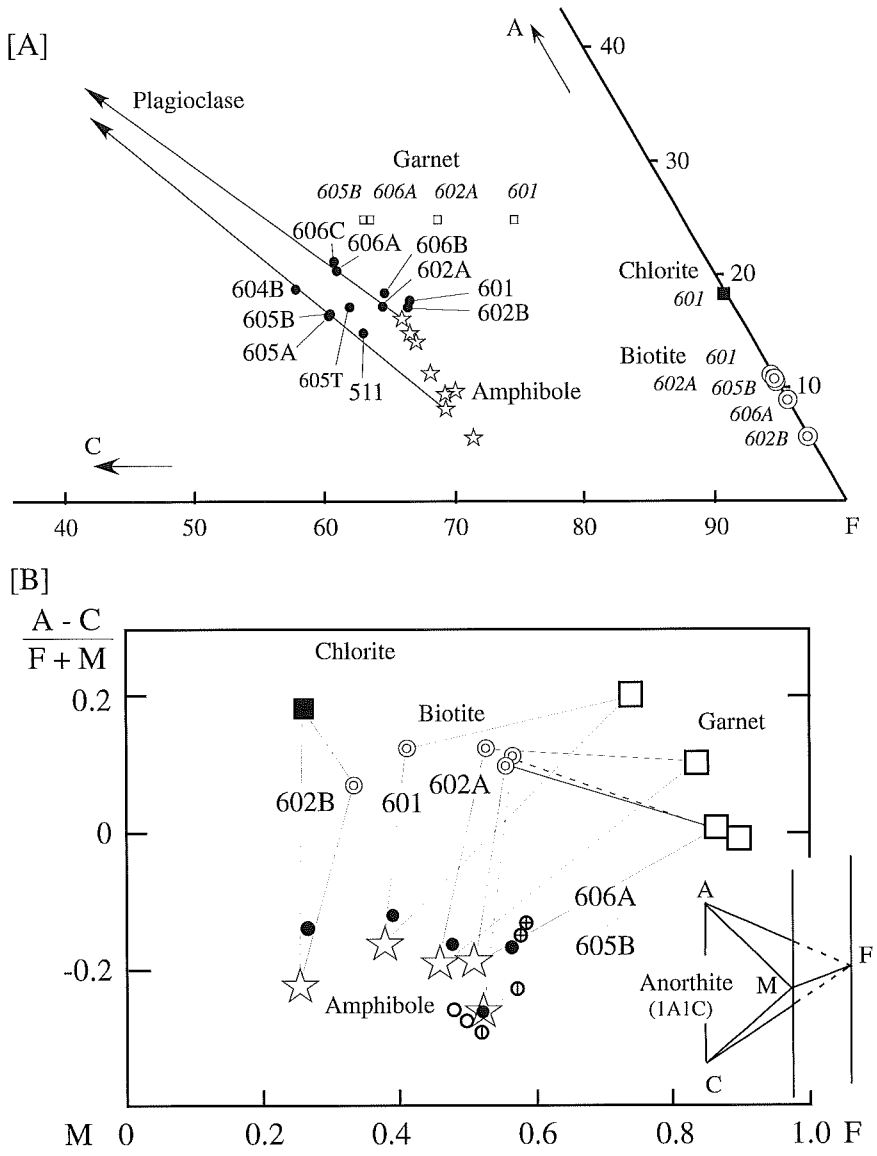

Fig. 4 ACF diagram for the amphibolite [A], and projection of phase relationships for amphibolites from quartz, H_2O and anorthite onto the plane that contains the F-M edge of the ACFM tetrahedron and that is parallel to the A-C edge [B]. Solid circles, stars, open squares, solid squares and double circles in [A] represent whole-rock, amphibole, garnet, chlorite and biotite compositions. Symbols in [B] are the same as those in [A], and open circles, open circles with vertical bar and open circles with cross represent whole-rock compositions of garnet-free, relict garnet-bearing and garnet amphibolites, for which mineral compositions were not measured.

compositions.

Sample 605B shows significant consumption of garnet by calcic plagioclase and edenitic hornblende. This type of garnet consumption may be attributable to hydration breakdown of garnet with modification of co-existing amphibole and plagioclase compositions in an open system (*e.g.* López Sánchez-Vizcaíno *et al.*, 2003).

Major garnet breakdown in 605B took place before late-stage deformation, whereas garnet in more Al-rich amphibolites such as sample 606A is better preserved. The composition of ferro-edenitic hornblende in the matrix of sample 605B lies close to the whole-rock composition on the projection plane (Fig. 4B). The enlargement of amphibole composition toward the A component diminishes the compositional field for the Gt+Hbl+Pl assemblage, and probably accelerates the garnet consumption in low Al amphibolite during the late stage of deformation.

The phase relationships in Fig. 4 emphasize the importance of whole-rock composition on the formation of mineral assemblages in amphibolites. The Al content, or more precisely the (A-C)/(F+M) value, is critical in determining whether the garnet+tschermakitic hornblende assemblage can develop in place of edenitic hornblende. At higher Fe/(Fe+Mg), the garnet-stability threshold decreases and garnet also accommodates more grossular. Thus, quite small variations in whole-rock composition can produce different mineral assemblages at a given pressure and temperature.

Contrasting concentrations of Sr in amphibolites

Figure 5 shows primitive mantle-normalized multi-element diagrams for garnet amphibolite (601, 602A, 606A, 606B and 606C), relict garnet-bearing amphibolite (605A, 605B and 605T) and garnet-free amphibolite (511, 602A and 604B). Figure 5 also includes normalized patterns of averages of N-type MORB, E-type MORB and OIB of Sun and McDonough (1989). The three types of amphibolite have similar normalized patterns and an affinity with E-type MORB in the abundance of high field strength elements. Sr, however, is significantly depleted in the garnet amphibolites.

Plagioclase is the main Sr-hosting mineral (*e.g.* Berlin and Henderson, 1968). Mineral assemblages during prograde metamorphism are not readily determined, because inclusions in garnet porphyroblasts are mainly quartz and plagioclase. However, mineral assemblages reported by Lee and Cho (1995) in lower-grade metabasites are often epidote-bearing, and Ep+Chl+Act+Ab+Qtz is a possible assemblage for pre-amphibolite grade metamorphism. Epidote can be a major host of Sr (Nagasaki and Enami, 1998). Sr inherited from plagioclase in E-type MORB protolith, therefore, can be hosted by epidote during albitization. Under intermediate-pressure conditions, epidote reacts with chlorite and quartz to form garnet and amphibole without significant production of plagioclase, as inferred from garnet amphibolite 606A (Fig. 2A). Since garnet and amphibole only can host small amounts of Sr (*e.g.* Yuhara *et al.*, 2002), the element can be readily leached by water-rich fluids liberated by dehydration breakdown of epidote and chlorite. In magnesian sample 602B, and possibly also in low-Al samples 511 and 604B, dehydration breakdown of epidote would have produced plagioclase, retaining Sr. In the case of relict garnet-bearing amphibolites 605A, 605B and 605T, Sr-hosting plagioclase (and possibly epidote) were present throughout metamorphism.

In other parts of South Korea, the presence of garnet-bearing, plagioclase-poor

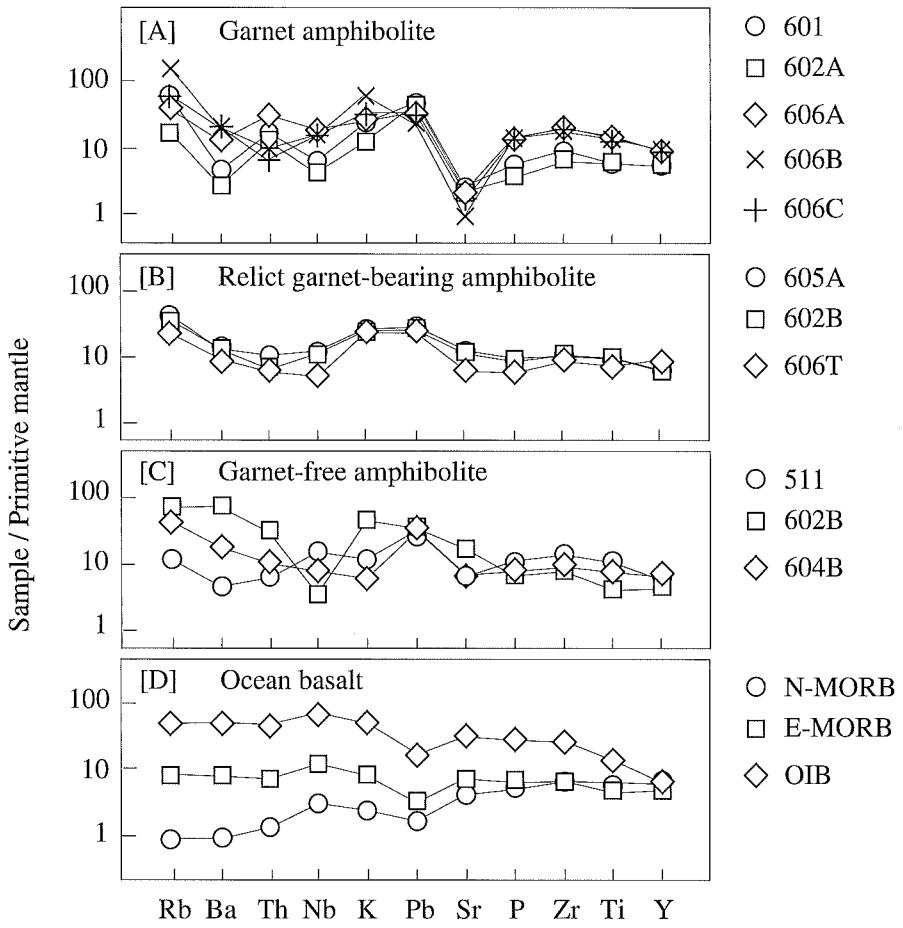

Fig. 5 Primitive mantle-normalized element abundances of [A] garnet amphibolite (samples 601, 602A, 606A, 606B and 606C), [B] garnet-bearing amphibolite (samples 605A, 605B and 605C) and [C] garnet-free amphibolite (samples 511, 602b and 604B). Normalization values from Sun and McDonough (1989). Also shown in [D] are primitive mantle-normalized element abundances of N-type MORB, E-type MORB and OIB of Sun and McDonough (1989).

assemblages in amphibolite localities has been attributed to polyphase metamorphism, where garnet was produced in the absence of plagioclase during earlier high-pressure, high-temperature metamorphism. The presence of matrix plagioclase is attributed to decompression to normal granulite or amphibolite-grade conditions. Such localities include relics of high-pressure garnet amphibolite in the Imjingang belt (Sajeev *et al.* 2009) and eclogitic remnants in the Hongseong and Bibong areas of the southwestern Gyeonggi massif (Oh *et al.*, 2005; Kim *et al.*, 2006). In the Chuncheon area, the co-existence of garnet-bearing and garnet-free amphibolites within outcrops is typical of such associations elsewhere; however, our interpretation favors differences in whole rock chemistry for garnet production, rather than polymetamorphism. The differing behavior of Sr between garnet-bearing and absent samples from a single outcrop

suggests that amphibolites did not experience high-pressure metamorphic conditions (eclogite-facies) that favor the formation of garnet-rich, plagioclase-free assemblages, because Sr would be hosted in stable phases such as epidote, paragonite and apatite (Glodny *et al.*, 2002).

SUMMARY

The amphibolites of the Gubongsan Group in the Chuncheon area have whole-rock chemistries that broadly match basaltic compositions with E-type MORB like characteristics. Mineral assemblages are divided into Gt+Hbl, relict Gt+Hbl, Hbl and Chl+Hbl types, with Pl+Qtz+Bt. Modal plagioclase is lowest in the rocks of the Gt+Hbl assemblage. The Chl+Hbl assemblage occurs in the most magnesian (Fe^{2+}/(Fe^{2+}+Mg)=0.26) sample. The garnet-bearing assemblages occur in Al-rich ferriferous rocks, and the garnet-free assemblages occur in Al-poor magnesian rocks. Element partitioning confirms an approach to chemical equilibrium within individual samples under a restricted range of P-T conditions. The distinct depletion in whole-rock Sr content of garnet amphibolites is ascribed to dewatering and breakdown of Sr-bearing minerals during progressive metamorphism. The geochemical signatures of the amphibolites indicate protolith formation in oceanic crust, as opposed to an island arc setting of the Baekdong metabasite in the southwestern part of the Gyeonggi massif (Oh *et al.*, 2004). Such magmatism may still be consistent with a continental rifting suggested by Kwon *et al.* (1995), if this led to the development of an ocean basin. There is, however, no evidence of the ocean development within granulitic basements of the Gyeonggi massif. Amphibolites and associated sub-granulitic gneisses are likely allochthons.

ACKNOWLEDGEMENTS

We thank Drs. Hyeoncheol Kim and Takeshi Imayama for the constructive review of the manuscript. Dr. Takenori Kato is acknowledged for discussions. This research was partially supported by the Ministry of Education, Science, Sports and Culture, Grant-in-Aid for Scientific Research (C), No. 21540471, 2009.

REFERENCES

Alirezaei, S. and Cameron, E.M. (2002): Mass balance during gabbro-amphibolite transition, Bamble Sector, Norway: implications for petrogenesis and tectonic setting of the gabbros. *Lithos*, **60**, 21–45.

Bence, A.E. and Albee, A.L. (1968): Empirical correction factors for the electron microanalysis of silicates and oxides. *Journal of Geology*, **76**, 382–403.

Berlin, R. and Henderson, C.M.B. (1968): A reinterpretation of Sr and Ca fractionation trends in plagioclase from basic rocks. *Earth and Planetary Science Letters*, **4**, 79–83.

Floyd, P.A. and Winchester, J.A. (1975): Magma type and tectonic setting discrimination using immobile elements. *Earth and Planetary Science Letters*, **27**, 211–218.

Glodny, J., Bingen, B., Austrheim, H., Molina, J. and Rusin, A. (2002): Precise eclogitization ages deduced from Rb/Sr mineral systematics: The Maksyutov complex, Southern Urals, Russia. *Geochimica et Cosmochimica Acta*, **66**, 1221–1235.

Jin, M.S., Shin, S.C., Kim, S.J. and Choo, S.H. (1993): Geochronology and thermal history of the Chuncheon granite in the Gyeonggi massif, South Korea. *Journal of the Petrological Society of Korea*, **2**, 122–129 (in Korean with English abstract).

Kato, T. (2005): New accurate Bence-Albee α-factors for oxides and silicates calculated from the PAP correction procedure. *Geostandards and Geoanalytical Research*, **29**, 83–94.

Kerric, R., Wyman, D., Hollings, P. and Polat, A. (1999): Variability of Nb/U and Th/La in 3.0 to 2.7 Ga Superior Province ocean plateau basalts: implications for the timing of continental growth and lithosphere recycling, *Earth and Planetary Science letters*, **168**, 101–115.

Kim, J., Cheong, C.-S., Lee, S.-R., Cho, M. and Yi, K. (2008): In-situ U-Pb titanite age of the Chuncheon amphibolite: Evidence for Triassic regional metamorphism in central Gyeonggi massif, South Korea, and its tectonic implication. *Geosciences Journal*, **12**, 309–316.

Kim, S.W., Oh, C.W., Williams, I.S., Rubatto, D., Ryu, I.-C., Rajesh, V.J., Kim, C.-B., Guo, J. and Zhai, M. (2006): Phanerozoic high-pressure eclogite and intermediate-pressure granulite facies metamorphism in the Gyeonggi Massif, South Korea: implications for the eastward extension of the Dabie-Sulu continental collision zone, *Lithos*, **92**, 357–377.

Kretz, R. (1983): Symbols for rock-forming minerals. *American Mineralogist*, **68**, 277–279.

Kwon, S.T., Cho, M., Jeon, E.Y., Lee, S.R. and Nakamura, E. (1995): Sm-Nd and Rb-Sr isotopic studies of the Chuncheon amphibolite. *Petrological Society of Korea* (abstract volume), **4**, 25.

Leake, B.E., Woolley, A.R., Arps, C.E.S., Birch, W.D., Gilbert, M.C., Grice, J.D., Hawthorne, F.C., Kato, A., Kisch, H.J., Krivovichev, V.G., Linthout, K., Laird, J., Mandarino, J., Maresch, W.V., Nickel, E.H., Rock, N.M.S., Schumacher, J.C., Smith, D.C., Stephenson, N.C.N., Ungaretti, L., Whittaker, E.J.W. and Youzhi, G. (1997): Nomenclature of amphiboles; report of the Subcommittee on Amphiboles of the International Mineralogical Association Commission on new minerals and mineral names. *Mineralogical Magazene*, **61**, 295–321.

Lee, S.M. (1987): Kyŏnggi metamorphic rock complex. In: Lee, D.S. (Ed.) Geology of Korea. Geological Society of Korea (Kyohak-Sa Publishing Co., Seoul), pp.351–359.

Lee, S.R. and Cho, M. (1995): Tectonometamorphic evolution of the Chuncheon amphibolite, central Gyeonggi massif, South Korea. *Journal of Metamorphic Geology*, **12**, 315–328.

López Sánchez-Vizcaíno, V., Gómez-Pugnaire, M.T., Azor, A. and Fernández-Soler, J.M. (2003): Phase diagram sections applied to amphibolites: a case study from the Ossa-Morena/Central Iberian Variscan suture (Southwestern Iberian Massif). *Lithos*, **68**, 1–21.

Ludden, J. Gélinas, L. and Trudel, P. (1982) Archean metavolcanics from the Rouyn-Noranda district, Abitibi Greenstone belt, Quebec. 2. mobility of trace elements and petrogenetic constraints. *Canadian Journal of Earth Science*, **19**, 2276–2287.

Morishita, T. and Suzuki, K. (1993): XRF analyses of the Mitsuhashi granite in the Shitara area, Aichi Prefecture. *Bulletin of Nagoya University Furukawa Museum*, No. 9, 77–90 (in Japanese with English abstract).

Mullen, E.D. (1983): $MnO/TiO_2/P_2O_5$: a minor element discrimination for basaltic rocks of oceanic environments and its implications for petrogenesis. *Earth and Planetary Science Letters*, **62**, 53–62.

Nagasaki, A. and Enami, M. (1998): Sr-bearing zoisite and epidote in ultra-high pressure (UHP) metamorphic rocks from the Su-Lu province, eastern China: An important Sr reservoir under UHP conditions. *American Mineralogist*, **83**, 240–247.

Oh, C.W., Choi, S.G., Song, S.H. and Kim, S.W. (2004): Metamorphic evolution of the Baekdong metabasite in the Hongseong area, South Korea and its relationship with the Sulu collision belt of China. *Gondwana Research*, **7**, 809–816.

Oh, C.W., Kim, S.W., Choi, S.G., Zhai, M., Guo, J. and Sajeev, K. (2005): First finding of Eclogite Facies metamorphic event in South Korea and its correlation with the Dabie-Sulu Collision Belt in China. *Journal of Geology*, **113**, 226–232.

Park, H.I., Chi, J.M., Chang, K.H. and Ko, I.S. (1974): Geologic map of Naepyeong sheet and explanatory text, pp. 1–13. Geological and Mineralogical Institute of Korea.

Pearce, J.A. and Cann, J.R. (1973): Tectonic setting of basic volcanic rocks determined using trace element analyses. *Earth and Planetary Science letters*, **19**, 290–300.

Pearce, J.A. and Norry, M.J. (1979): Petrogenetic implications of Ti, Zr, Y and Nb variations in

volcanic rocks. *Contributions to Mineralogy and Petrology*, **69**, 33–47.

Sagong, H., Cheong, C.-S. and Kwon, S.T. (2003): Paleoproterozoic orogeny in South Korea: evidence from Sm-Nd and Pb step-leaching garnet ages of Precambrian basement rocks. *Precambian Research*, **122**, 275–295.

Sajeev, K., Jeong, J., Kwon, S., Kee, W.-S., Kim, S.W., Komiya, T., Itaya, T., Jung, H.-S. and Park., Y. (2009): High P–T granulite relics from the Imjingang belt, South Korea: Tectonic signifcance. *Gondwana Research*, **17**, 75–86.

Shervais, J.W. (1982): Ti-V plots and the petrogenesis of modern and ophiolitic lavas. *Earth and Planetary Science Letters*, **59**, 101–118.

Sun, S.S. and McDonough, W.F. (1989): Chemical and isotopic systematics of oceanic basalts: implications for mantle composition and processes. In Saunders, A.D. and Norry, M.J. (Eds) Magmatism in Ocean Basins. Geological Society of London Special Publication 42, 313–345.

Suzuki, K. (2009): CHIME dating and age mapping of monazite in granulites and paragneisses from the Hwacheon area, Korea: implications for correlations with Chinese cratons. *Geosciences Journal*, **13**, 275–292.

Suzuki, K., Tsuboi, M. and Cho, M. (2002): CHIME dating of metamorphic rocks from the Gyeonggi massif in the Chuncheon area, South Korea. Abstract (O-56) of the 109th annual meeting of the Geological Society of Japan. 28 (in Japanese).

Yamamoto, K. and Morishita, T. (1997): Preparation of standard composites for the trace element analysis by X-ray fluorescence. *Journal of the Geological Society of Japan*, **103**, 1037–1045 (in Japanese with English abstract).

Yuhara, M., Miyazaki, T., Ishioka, J., Suzuki, S., Kagami, H. and Tsuchiya, N. (2002): Rb-Sr and Sm-Nd mineral isochron ages of the metamorphic rocks in the Namaqualand metamorphic complex, South Africa. *Gondwana Research*, **5**, 771–779.